Ergodic and non-ergodic phase transitions in globular protein suspensions

Amit M. Kulkarni,† Narendra M. Dixit and Charles F. Zukoski*

Department of Chemical Engineering, University of Illinois at Urbana-Champaign, 114, Roger Adams Laboratory, 600 S. Mathews Avenue, Urbana IL-61801, USA. E-mail: czukoski@uiuc.edu

Received 8th May 2002, Accepted 7th June 2002
First published as an Advance Article on the web 16th December 2002

The equilibrium and nonequilibrium phase behavior of a protein suspension is investigated as a function of strength of interparticle attraction and protein concentration. The equilibrium phase behavior suggests that the range of the particle attractions is a small fraction of their diameter. At volume fractions and strengths of attractions smaller than those characterizing the spinodal of a metastable fluid–fluid transition, the suspensions gel before they crystallize. At higher volume fractions and lower strengths of attraction, gels are formed first from which crystals nucleate over a period of time. However, at higher strength of attraction, crystals form first at lower volume fractions while gels are observed at higher volume fractions. We hypothesize that this behavior results from the competition between the rates of gelation and crystal nucleation. The location of the gel line is well predicted by mode coupling theories adapted for low volume fractions and square well fluids. At low strength of attraction, the gel line occurs at small supersaturations suggesting gels will be seen before nucleation. However, at higher strengths of attraction the gel line occurs at greatly increased supersaturations such that crystal nucleation can occur before the gel line is crossed. That mode coupling theories should predict gelation when crystallization does not intervene is tested by investigating the gel dynamics.

I. Introduction

Nanoparticle suspensions experiencing attractions undergo a series of phase transitions as the strength of attraction and particle concentration are increased. When the range of the attraction is of the order of the size of the particle, equilibrium fluid–fluid and fluid–crystal phase transitions are observed.[1] However when the range of the attraction is small compared to the size of the particle, fluid–fluid phase transitions are metastable with respect to fluid–crystal transitions for all dimensionless temperatures. The location of the critical point relative to the fluid–crystal phase boundary at the critical concentration is a function of attractive well width and anisotropy of the particle interactions.[2] In some nanoparticle systems gels are formed.[3–8] The differences in the events giving rise to crystals or gels are poorly understood. Here, we discuss the gelation and crystallization of a protein system. In this system these transitions occur over time scales allowing accurate determination of changes in the system dynamics.

† Present address: General Electric Company, Global Research Center, Schenectady, NY 12301, USA.

The equilibrium phase behavior of nanoparticles has seen extensive study over the past decade, primarily with the aim of understanding protein crystallization.[9–13] Comparison of experimental and theoretical phase behavior suggests most nanoparticle systems show equilibrium phase behavior characteristic of particles experiencing attractions that have a range much smaller than the particle size. The signature for this aspect of the particle interaction energy is the existence of only two thermodynamically stable phases: fluid and crystals. Metastable fluid–fluid transitions are seen when these systems are quenched rapidly below the solubility boundary. Unlike pure molecular systems, the strength of attraction can be manipulated by changes in solution conditions such that the phase diagram can be explored at constant temperature. For protein systems, there is no *a priori* method of determining the strength of attraction. As a result, understanding solution thermodynamic properties and comparisons between different protein systems and different solvent conditions requires that the interaction potential be characterized.

One method to provide an experimental scaling of the strength of attraction is to measure the second virial coefficient of the osmotic pressure, B_2. The second virial coefficient is determined by measuring the concentration dependence of the static structure factor, $S(q)$, where q is the magnitude of the scattering vector. The zero angle limit, $S(0) = (\mathrm{d}P/kT\mathrm{d}\rho)^{-1}$, where kT is the product of the absolute temperature and the Boltzmann's constant, P is the osmotic pressure, and ρ is the particle number density. In the low volume fraction limit, for spherical particles,

$$\frac{1}{kT}\frac{\mathrm{d}P}{\mathrm{d}\rho} = 1 + 8\frac{B_2}{B_2^{\mathrm{HS}}}\phi + \vartheta(\phi^2) \tag{1}$$

where $B_2{}^{\mathrm{HS}} = (2\pi/3)\sigma^3$ is the hard sphere second virial coefficient, with σ, the sphere diameter, and $\phi = (\pi/6)\rho\sigma^3$ is the particle volume fraction. For particles interacting with centro-symmetric pair potentials, the scaled second virial coefficient, $B_2/B_2{}^{\mathrm{HS}}$ is related to the particle interaction potential $U(r)$ through:

$$\frac{B_2}{B_2^{\mathrm{HS}}} = 3\int_0^\infty (r/\sigma)^2\left(1 - \mathrm{e}^{-U(r)/kT}\right)\mathrm{d}(r/\sigma) \tag{2}$$

Using $B_2/B_2{}^{\mathrm{HS}}$ as a dimensionless temperature, generalized phase diagrams have been developed showing that broad classes of nanoparticles have very similar equilibrium phase behavior with the largest differences arising in the magnitude of the scaled second virial coefficient at the metastable fluid–fluid critical point, $(B_2/B_2{}^{\mathrm{HS}})_{\mathrm{c}}$.[2,9]

Gelation of suspensions has been studied primarily with themo-reversible gels[6–8,14] and depletion aggregated systems where increases in attraction lead to non-ergodic states.[3–5,15,16] Recent experiments suggest two distinct routes to gelation. In the first ergodic gel system, particles are aggregated into clusters, where particles within a cluster have fixed averaged positions relative to other particles in the cluster, but the centers of mass of the clusters themselves remain ergodic.[15] Upon increasing the particle concentration, the number density of the clusters increases and the clusters eventually jam to produce a space-filling gel. The second, more commonly reported gel involves the trapping of individual particles in dynamic cages formed by their neighboring particles. These gels have been likened to glasses observed in dense colloidal suspensions.[16]

For hard sphere colloidal glasses, predictions of mode coupling theories, MCT, have shown excellent agreement with measurements of the intermediate scattering function,[17] providing support for the mode coupling description of cage formation being the origin of the glass transition. MCT provides a self-consistent method for determining the dynamics of particles that spend longer and longer times trapped in cages, formed by their neighboring particles, as the volume fraction is increased. For the particles to diffuse over distances comparable to their sizes, these cages must break open. As the particle concentration is increased, cage breaking becomes less probable as it requires the cooperative rearrangement of many particles which are themselves trapped in similar cages. At the "idealized" glass transition, diffusion becomes impossible causing complete structural arrest into a non-ergodic state.

Mode coupling theories have recently been extended to attractive systems where non-ergodic transitions are predicted at volume fractions well below that characterizing glass formation for hard spheres ($\phi_{\mathrm{glass}} \sim 0.58$).[18] This approach explicitly ignores density fluctuations by assuming

$S(q) = 1$ for all q. Loss of ergodicity occurs due to increases in bond strength. This model has recently been shown to provide a good description of gelation of hard sphere particles experiencing depletion attractions when the depletant size is much smaller than the particle size.[16] Comparison of conditions giving rise to gelation requires that pair interactions be characterized. Again, for nanoparticles, B_2/B_2^{HS} offers a convenient basis for making the comparison.

Here we characterize the equilibrium phase diagram of a nanoparticle system that shows a gel transition in suspensions supersaturated with respect to the fluid–crystal phase boundary but at strengths of attraction and volume fractions less than those characterizing the metastable critical point of the fluid–fluid transition. At small strengths of attraction, crystal nucleation is slow, such that gels form before crystals nucleate. Under these conditions, we find that the simplified version of the mode coupling theory[18] captures the location of the gel line on the protein phase diagram. The dynamics of density fluctuations within the gels are also well described by the mode coupling theory.

At larger strengths of attraction, the driving force for crystallization increases and crystals nucleate faster than gels can form. This observation raises important questions about the competition between gelation and crystallization in attractive nanoparticle systems. Using, as a basis of comparison, literature calculations for square well systems we suggest that the competition is dictated by the interplay of static percolation, the gel transition predicted by mode coupling theory, and the dynamics of crystal nucleation.

In Section II, we describe our experimental methods, and discuss the phase behavior of lysozyme in a phosphate buffer system in Section III. The dissipation of density fluctuations is discussed in Section IV where we demonstrate agreement with MCT predictions. We discuss the competition between gelation and crystallization in Section V, and draw conclusions in Section VI.

II. Experimental

The experimental system studied is composed of the protein lysozyme (diameter $\sigma = 3.4$ nm)[19] suspended in a pH 7.0 sodium phosphate buffer at an ionic strength of 0.6 M. Solubilities, ϕ_{sat}, for lysozyme were measured by allowing crystals to grow in suspensions held at a fixed temperature for several months. The solubility is taken as the steady state protein concentration in solution above the crystals. By measuring the second virial coefficient of the protein solutions, we are able to construct a generalized phase diagram where B_2/B_2^{HS} is taken as a measure of the strength of attraction in the place of a dimensionless temperature. This process is facilitated by the measurement of B_2 as a function of temperature in dilute solutions where the intensity of the scattered light, I, normalized to the particle concentration, c was a linear function of c (*i.e.*, c/I *versus* c was a linear function of c with intercept proportional to the (lysozyme molecular weight)$^{-1}$ and the slope proportional to B_2). (See ref. 20 for detailed discussion of measurement techniques.) These measurements were made at lysozyme concentrations well below the solubility limit. The generalized phase diagram is presented in Fig. 1, with the experimental solubilities shown as solid triangles.

Cloud point measurements were made by rapidly reducing the suspension temperature and observing the temperature where the suspension became turbid. This was done with an accuracy of $\pm 0.2\,^{\circ}$C. Again by knowing the temperature dependence of B_2, we plot cloud point measurements on the generalized phase diagram (solid squares). The critical point occurs at $(B_2/B_2^{HS})_c = -2.7$.

The osmotic compressibility, $dP/kTd\rho$, was measured at different concentrations of lysozyme in 0.6 M sodium phosphate buffer, pH 7.0 at a temperature of 10 °C. Lysozyme concentrations were varied from 5 mg ml^{-1} to 90 mg ml^{-1}. The samples were equilibrated at 10 °C for 30 min (sufficiently smaller than the time required for forming gels or crystals discussed below) prior to the measurement. The measurements were made using static light scattering methods[20] and are presented in Fig. 2.

The dynamics of both ergodic (fluid-like) and non-ergodic (gel) samples were characterized by measurements of the intermediate scattering function, $f(q,\tau)$, using dynamic light scattering (DLS). DLS measurements yield the normalized time-averaged auto-correlation function (ACF) of the scattered intensity,[17]

$$g_T^{(2)}(q,\tau) = \frac{\langle I(q,0)I(q,\tau)\rangle_T}{\langle I(q)\rangle_T^2} \tag{3}$$

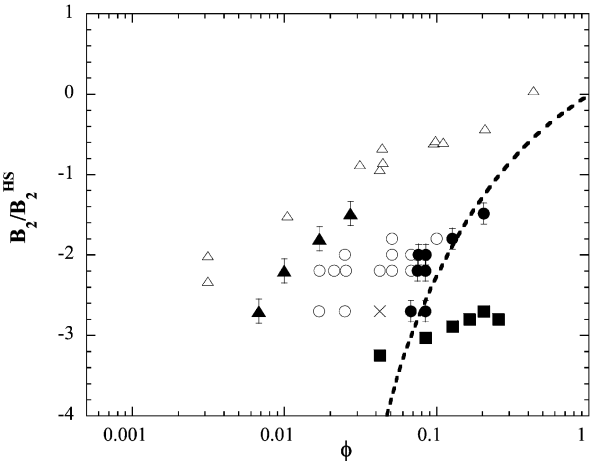

Fig. 1 Generalized phase diagram for the lysozyme/phosphate system. Solid triangles and squares represent the experimental solubility and the liquid–liquid boundary, respectively, for the lysozyme/phosphate system studied here. Solubility points from other lysozyme studies[13] are shown as open triangles. Open circles represent fluid-like suspensions, where scattered light intensity and diffusivity were time invariant. The cross denotes suspension where crystals are first observed. Solid circles represent those suspensions where gels form at short times. The long dashed line represents the MCT bond formation line at $\Delta = 0.08$.

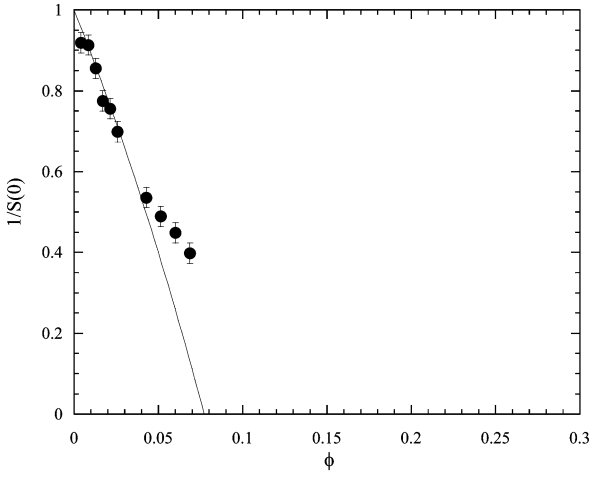

Fig. 2 Inverse static structure factor, $1/S(0) = \mathrm{d}P/kT\mathrm{d}\rho$ as a function of volume fraction for lysozyme in a 0.6 M sodium phosphate buffer solution at pH 7.0 at 10 °C. The solid line represents square well equation of state predictions at $\Delta = 0.08$ ($\varepsilon/kT = 3.6$).

where $q = (4\pi n/\lambda)\sin(\theta/2)$, is the scattering wave vector, with λ, the wavelength of incident light, n, the refractive index of the medium, and θ, the scattering angle. τ is the delay time in the correlation function, and $\langle\ \rangle_T$ represents a time average over the duration of the experiment, T. For an ergodic sample, the time average is equal to its ensemble average $\langle\ \rangle_T$ is equal to its ensemble average, $\langle\ \rangle_E$, *i.e.*,

$$g_T^{(2)}(q,\tau) = g_{\mathrm{E}}^{(2)}(q,\tau) \tag{4}$$

and the Siegert relationship,[17]

$$g_{\mathrm{E}}^{(2)}(q,\tau) = 1 + c[f(q,\tau)]^2 \tag{5}$$

is used to obtain $f(q,\tau)$ from measurements of $g_T^{(2)}(q,\tau)$. Here c is an experimental constant proportional to the ratio of the coherence area to the detector area ($0 < c < 1$). For monodisperse, spherical scatterers, the dynamic structure factor is given by,

$$f(q,\tau) = \exp(-Dq^2\tau) \tag{6}$$

where D is the translational gradient diffusion coefficient, which, in the dilute limit, corresponds to the Stokes–Einstein diffusivity, $D_0 = kT/3\pi\eta\sigma$, with η, the solvent viscosity. The diffusivities obtained from fits of eqn. (6) to the $f(q,\tau)$ data on ergodic samples of increasing particle volume fractions are presented in Fig. 3.

For non-ergodic samples, where $g_T^{(2)}(q,\tau) \neq g_E^{(2)}(q,\tau)$, the unnormalized ACF, $\langle I(q,0)I(q,\tau)\rangle_T$, and the average scattered intensity, $\langle I(q)\rangle_T$, were measured for different sub-ensembles in a sample, and averaged to determine $g_E^{(2)}(q,\tau)$:[14,17]

$$g_{\mathrm{E}}^{(2)}(q,\tau) = \frac{\left\langle \langle I(q,0)I(q,\tau)\rangle_T \right\rangle_n}{\left\langle \langle I(q)\rangle_T \right\rangle_n^2} \tag{7}$$

where n indicates the number of measurements over which the average is taken. The Seigert relationship (eqn. (5)) was then used to determine $f(q,\tau)$. Using this technique, $g_E^{(2)}(q,\tau)$ did not change appreciably for $n \geqslant 8$. Hence, for all the non-ergodic samples studied here, $f(q,\tau)$ was obtained for $n = 10$. The results are presented in Fig. 4–6 and are discussed in Section IV.

Experiments to determine the behavior of the suspension as a function of supersaturation were carried out by making suspensions at the desired volume fractions and then quenching rapidly to the desired temperatures. For supersaturations, ϕ/ϕ_{sat}, less than 6, no crystals or gels were observed for up to six months. Indeed as discussed below, the intermediate scattering function was well described by a single exponential relaxation curve with a time invariant relaxation time scaling as q^2. Systems showing this behavior are shown as open circles in Fig. 1. For larger volume fractions at temperatures of 10–18 °C ($B_2/B_2^{\mathrm{HS}} > -2.5$), upon quenching, the protein suspensions formed transparent gels over a period of a day or two. Gelation was indicated by the suspensions no longer flowing upon tipping the test tube, by an increase in scattered light intensity with time,

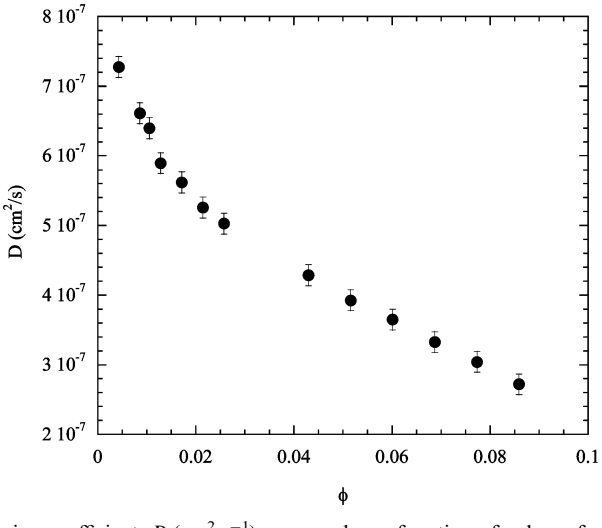

Fig. 3 Gradient diffusion coefficient, D (cm^2 s^{-1}) measured as a function of volume fraction of lysozyme in a 0.6 M sodium phosphate buffer solution at pH 7.0 at 10 °C.

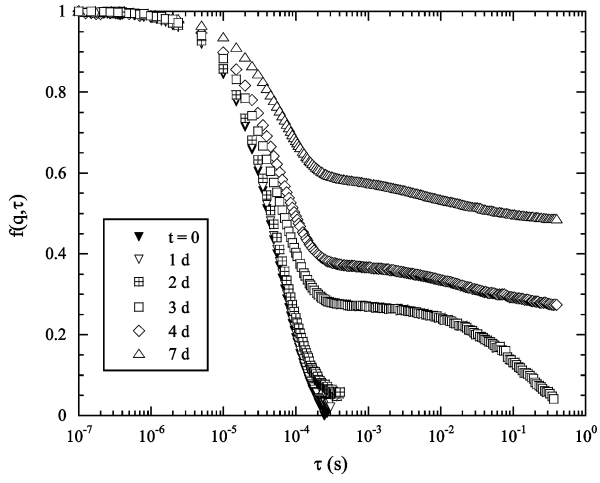

Fig. 4 Dynamic structure factors representing the time evolution or aging of lysozyme solution at volume fraction $\phi = 0.076$ ($c = 90$ mg ml^{-1}) at 11 °C at $q = 23$ μm^{-1}.

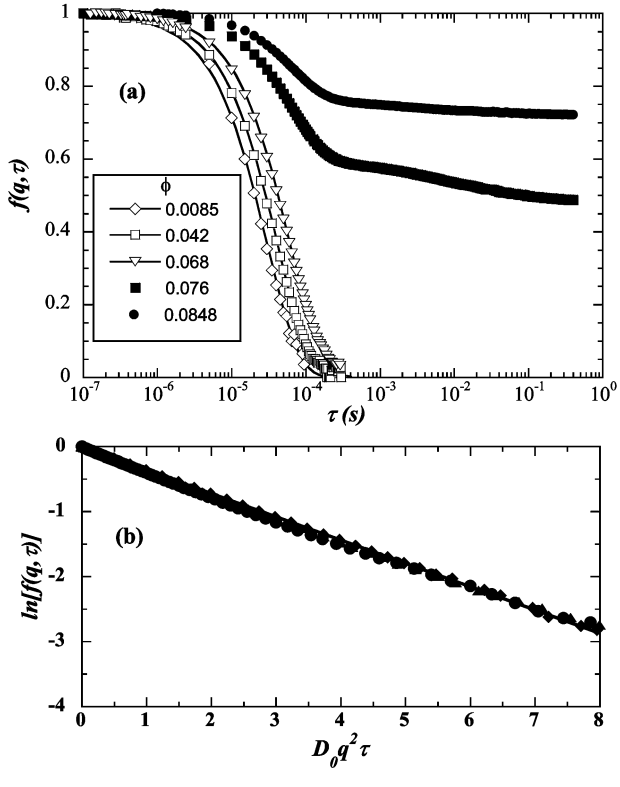

Fig. 5 (a) Dynamic structure factor as a function of the delay time for different lysozyme concentrations in the phosphate buffer at $B_2/B_2^{HS} = -2.2$ and at wave vector, $q = 23$ μm^{-1}. The solid lines through the data are single exponential fits. (b) Scaling of the dynamic structure factors for $\phi/\phi_g = 0.89$ showing single exponential dynamics with relaxation times which scale as q^2. Circles, triangles, and diamonds represent data at $q = 5.7$, 13.8, and 23 μm^{-1}, respectively. The solid line is a linear fit to the data.

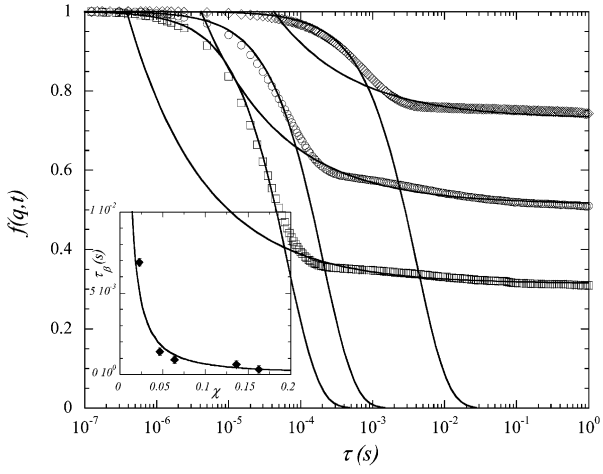

Fig. 6 Dynamic structure factors for $\phi = 0.0848$ ($B_2/B_2^{HS} = -2.0$) at three wave vectors. The solid lines represent two fits at each q: a short time exponential decay (eqn. (11)) and a long time power law decay (eqns. (12) and (13)). The inset shows the relaxation time τ_β as a function of separation parameter, χ, where τ_β is obtained from the MCT fits to $f(q,\tau)$ data measured at different concentrations and temperatures (not shown).

and by the growth of a non-zero long time asymptote to the intermediate scattering function. Over periods of many days to several weeks, crystals formed from these gels. Over a period of months the gels disappeared and the system consisted of crystals in equilibrium with a fluid at protein concentration ϕ_{sat}. All systems that first gelled upon quenching are shown as solid circles in Fig. 1. At a temperature of 5 °C ($B_2/B_2^{HS} = -2.7$), crystals nucleated at lower volume fractions (but still $\phi/\phi_{sat} > 6$), shown by a cross in Fig. 1. However as ϕ increased, upon quenching, gels were formed first and then crystals nucleated within the gels (shown by the solid circle at the same B_2/B_2^{HS}). We also note that for a fixed B_2 as ϕ is increased above the gel volume fraction, ϕ_g, crystals nucleate more and more rapidly from the gelled state. In addition if ϕ ($> \phi_g$) is fixed and B_2 is decreased, crystals nucleate more quickly.

III. Discussion of phase behavior

Several intriguing features emerge from an examination of the experimental phase diagram shown in Fig. 1. First, the particles have a phase diagram where the critical point lies in the fluid–crystal coexistence region (*i.e.*, the fluid–fluid phase transition is metastable with respect to the fluid–crystal phase transition). Comparisons with the phase behavior predicted using a variety of interaction potentials suggest this behavior results from particles experiencing short-range attractions.[3–7,13] The system we investigate clearly falls into this class of materials. We note, however, that the value of B_2/B_2^{HS} at the metastable critical point (−2.7) is significantly lower than the range of values predicted by mean field theories assuming centrosymmetric attractions between the particles where $(B_2/B_2^{HS})_c > -1.65$.[2] Models assuming anisotropic interactions, on the other hand, are able to predict large negative values of $(B_2/B_2^{HS})_c$ as observed here, suggesting that the lysozyme particles in the present system experience strong anisotropic attractions.[2,12]

The second point we note is that crystallization is not observable in any reasonable time frame for supersaturations up to 6. In other systems, *e.g.*, hard sphere colloidal suspensions, crystallization is seen in a few minutes at supersaturations as low as 1.05.[21] We speculate that the slow nucleation kinetics is a consequence of the anisotropic nature of the particle interactions. For crystals to nucleate, not only do the particles have to aggregate, but they also have to orient themselves appropriately in order to form bonds. The latter process can be slow, especially if it requires the cooperative reorientation of many particles.

The third point we emphasize is that the conditions under which gelation occurs here are widely separated from the cloud point curve (commonly taken as the spinodal of the metastable fluid–fluid

transition). Previous studies, both experimental and theoretical, on particles experiencing adhesive hard sphere interactions, suggest that gelation is intimately linked to spinodal decomposition.[6,7,14,22] Using a different approach, however, a recent theoretical study on particles experiencing longer ranged interactions suggests that gelation is decoupled from spinodal decomposition and that the relative locations of the gel line and the critical point can be altered by varying the range of the attractions.[23] This equation of state approach assumes gelation occurs at volume fractions and strengths of attraction above the static percolation boundary. In agreement with these predictions, mode coupling theories for the loss of ergodic dynamics are based on liquid state suspension structures and are only applicable outside the spinodal. For the lysozyme–phosphate system, gelation and fluid–fluid phase separation are widely separated suggesting that these two phenomena are decoupled.

The fourth feature of interest in the phase behavior presented in Fig. 1 is the long time behavior of the system. Despite the slow crystal nucleation kinetics, we note that at very long times (months), crystals result in all gelled systems. The gels are thus truly transient. This observation indicates that despite extremely long relaxation times these gels seek the system's lowest free energy state. We note that the ability of apparently non-ergodic systems to sample lower free energy states has also been seen in hard sphere suspensions, where, upon avoiding gravity driven effects, crystals nucleate in hard sphere glasses.[24] This points to the existence of structural relaxation mechanisms not accounted for in mode coupling theories.

The fifth aspect of Fig. 1 to which we call attention is that for $B_2/B_2^{HS} > -2.5$, increasing the particle volume fraction above the solubility boundary leads to gelation. However, at larger strengths of attraction (more negative B_2/B_2^{HS}), increasing the volume fraction at fixed B_2 results in crystallization. These observations suggest that there is a competition between the processes giving rise to crystallization and those giving rise to gelation. In other systems that gel, increasing the strength of attraction at a given volume fraction or increasing the volume fraction at a given strength of attraction increases the tendency of the suspension to form gels.[3,10,16] In the lysozyme system studied here, while increasing the volume fraction at any strength of attraction increases the tendency to form gels, increasing the strength of attraction at a given volume fraction increases the tendency of the system to form crystals.

To understand the gelation behavior we turn to recent mode coupling models that have been developed for systems with attractions in the limit of low volume fractions. This approach results in a simple analytical condition for the gelation of spherical particles interacting with square well attractions of range Δ.[25] For square well systems the particles are assumed to have an interation energy $U(r)$:

$$\frac{U(r)}{kT} = \begin{cases} \infty & r \leq \sigma \\ -\varepsilon/kT & \sigma < r \leq \sigma(1+\Delta) \\ 0 & r > \sigma(1+\Delta) \end{cases} \tag{8}$$

where r is the center-to-center separation of a pair of particles, ε, the strength of the attraction between the particles of diameter σ, and Δ, the range of the attraction. Here, kT is the product of Boltzmann's constant and the absolute temperature. For the square well potential, eqn. (2) yields:

$$\frac{B_2}{B_2^{HS}} = 1 - (e^{\varepsilon/kT} - 1)((1+\Delta)^3 - 1) \tag{9}$$

Assuming that density fluctuations (*i.e.*, $S(q) = 1$) are not important in determining the location of the gel line Bergonholtz *et al.*[25] derive the flowing expression for the location of the MCT gel line:

$$12\Delta\varphi(\exp(\varepsilon/kT) - 1)^2/\pi^2 = 1.42 \tag{10}$$

The non-equilibrium behavior arises solely from the strength of attraction growing to a sufficient size that once in contact, pairs of particles can no longer separate.[25] Converting the well depth ε/kT in eqn. (10) to B_2/B_2^{HS} using eqn. (9), we plot in Fig. 1 the MCT gel line (dashed line) for $\Delta = 0.08$. Note that the MCT line lies close to the experimental gel line for all B_2/B_2^{HS} where gelation is observed. This remarkable agreement prompted us to test the main predictions of MCT regarding the dynamics of gelation, which we report in the following section.

IV. Dynamics of structural relaxation

The ability of MCT to capture the observed gel line suggests important differences in the mechanism of gelation observed in our system from the mechanism observed by Segre *et al.*,[15] who argue that stable fractal aggregates form in suspensions with volume fractions smaller than the gel volume fraction. Increasing the volume fraction increases the aggregate number density. Eventually, the clusters become densely packed and percolate to form gels. In contrast, the gel transition predicted by MCT involves the caging of individual particles and not the percolation of clusters. Increasing the particle volume fraction leads to tighter cages and slower dynamics. We note that in the absence of clusters, gelation requires the existence of a percolated network of particles that spans space. Gelation thus occurs when the relaxation of percolated structures requires times longer than experimental timescales. A test of the ability of MCT to capture the gelation of this system comes from investigating the relaxation of density fluctuations before and in the gelled state. Here, we provide such a comparison.

We begin with the dynamics of ergodic suspensions in Fig. 3, where we present collective diffusivities as a function of volume fraction at a temperature of 10 °C ($B_2/B_2^{HS} = -2.2$). The diffusivity decreases with increasing volume fraction. The reported diffusivities were measured from the intermediate scattering function, $f(q,\tau)$, where $f(q,\tau)$ has the form $\exp(-q^2 D\ \tau)$. Note that the protein solubility $\phi_{sat} = 0.01$ at this temperature, indicating that, well into the supersaturated region, density fluctuations decay in a diffusive manner with a single decay constant indicative of a system consisting of a uniform particle size distribution. This is emphasized in Fig. 5(b) where $\ln[f(q,\tau)]$ is plotted as a function of $Dq^2\tau$ for $\phi = 0.068$ at $q = 5.7$, 13.8 and 23 μm^{-1}. Even at this volume fraction, where $\phi/\phi_g = 0.89$ and $\phi/\phi_{sat} = 6.5$, the decay in $f(q,\tau)$ is time invariant for a period of several months. However, for $\phi/\phi_{sat} > 6.5$, $f(q,\tau)$ evolved over a period of hours and days to a state where in the limit of large τ, $f(q,\tau)$ did not decay to zero, indicative of a non-ergodic system. An illustration of the time evolution of $f(q,\tau)$ at $\phi = 0.076$ ($\phi/\phi_{sat} = 7.3$) is given in Fig. 4.

From the data in Figs. 3 and 4, we conclude, in the following manner, that the dynamics of the system is slow. First, the collective diffusivity can be written as $D/D_0 = H(q)/S(q)$ where D_0 is the zero volume fraction diffusivity and $H(q)$ is a wave vector dependent hydrodynamic factor.[1] In the low volume fraction, $q = 0$ limit, $D/D_0 = 1 + D_2\phi$ where $D_2 = 8B_2/B_2^{HS} + K_2$. Here K_2 is the hydrodynamic factor associated with the sedimentation velocity of particles in a uniform suspension, $u = u_0(1 + K_2\phi)$, where u_0 is the sedimentation velocity in the limit as ϕ goes to zero. K_2 can be calculated from a knowledge of the hydrodynamic interactions of settling particles in the pair limit and by assuming that in this limit, the pair distribution function can be written as $g(r) = \exp(-U(r)/kT)$.[1]

Using the measured value of B_2/B_2^{HS} (−2.2) for the data in Fig. 4, and assuming a square well attraction with $\Delta = 0.08$ and ε/kT required to yield the measured B_2, we calculate $K_2 = 4.7$, (*i.e.*, in the presence of attractions particles settle faster than in the absence of attractions where $K_2 = -6.5$) yielding $D_2 = -12.9$. The measured value of D_2 is −18.8, indicating that diffusion is slower than can be predicted with the standard models. Such behavior has been seen in other systems[26,27] and may be indicative that strong attractions give rise to non-equilibrium behavior observable in the pair limit even when $0.02 < \sigma q < 0.1$. That $f(q,\tau)$ is time invariant over periods of months and decays in a purely diffusive manner characterized by a single relaxation time even in supersaturated systems indicates that diffusion is anomalously slow and that clusters are not present at concentrations detectable by dynamic light scattering. These results are surprising as classical nucleation theories suggest that at supersaturations of 3–6, the critical nucleus size is a single particle and nucleation is diffusion limited.[28] Again, there is no evidence of microscopic or macroscopic crystals in this volume fraction range over periods of months.

The approach to a non-ergodic state is shown in Fig. 4 where the steady state non-ergodic $f(q,\tau)$ is established over a period of several days. Again if the system gelled by diffusion limited aggregation, one would expect clusters to form at the Smoluchowski rate characterized by a half time for loss of monomers, $t_{1/2} = \pi\eta\sigma_3/8\phi kT = 5.2 \times 10^{-8}$ s[1]. The slow gelation kinetics and the lack of angular dependence in the scattered light intensity through the ergodic–non-ergodic transition suggest that the gelation process occurs through a reaction limited mechanism.

Shown in Fig. 5(a) are steady state dynamic light scattering curves showing relaxation in the dynamic structure factor at five concentrations for $B_2/B_2^{HS} = -2.2$. Under these conditions, the

system gels before crystals are observed. For $\phi < \phi_g = 0.074$, the correlation functions are independent of the macroscopic time, t. For $\phi > \phi_g$, as shown in Fig. 4, a metastable steady state is reached after two or three days when the system has gelled. The gels are clear and space filling. Over time, crystals grow out of the gels. Here we focus on the dynamics of the "pseudo-steady state" gel (as shown in Fig. 5). When the dynamics are non-ergodic, $f(q,\tau)$ is obtained, as described in Section II.[17] In the non-ergodic pseudo-steady state, $f(q,\tau)$ starts as a single exponential at short delay times, shows hindered diffusion at intermediate times and decays in two distinct steps to a finite plateau value at delay times of 1 s (Fig. 5(a)). This unusual two-step decay, as discussed below, may be attributed to the anisotropic nature of particle interactions.

We compare our results with predictions of the MCT, which describes the dynamics of the system upon approaching a critical concentration, ϕ_g, at which a dynamic instability characterizes the ergodic to non-ergodic transition.[18,25] The approach to the transition from the fluid side is accompanied by the emergence of two distinct relaxation processes, the α and the β processes, whose time scales, τ_α and τ_β diverge with non-universal exponents. The very short time τ_0 characterizes the time scale of local or microscopic particle motion about a fixed location, where,

$$f(q,\tau) = \exp(-\Gamma\tau) \quad \tau \ll \tau_0 \tag{11}$$

For intermediate times $\tau_0 \ll \tau \ll \tau_\alpha$, the dynamics are governed by the β process for which the predicted dynamic structure has the form,

$$f(q,\tau) = f_c(q) + h(q)\chi^{1/2} G_\pm(\tau/\tau_\beta) \quad \tau_0 \ll \tau \ll \tau_\alpha \tag{12}$$

where $f_c(q) = f(q,\tau \to \infty) \neq 0$, is the non-ergodicity parameter which represents the fraction of the structure that is arrested at concentration ϕ_g. $G_\pm$ is a universal master function or β-correlator given as,

$$\begin{aligned} G_+(\tau/\tau_\beta) &= (\tau/\tau_\beta)^{-a} \\ G_-(\tau/\tau_\beta) &= -B(\tau/\tau_\beta)^b \end{aligned} \tag{13}$$

where B is a constant of the order of 1, and a, b are non-universal exponents. The subscript $\pm$ indicates the sign of the separation parameter, χ, defined by $\chi = (\phi - \phi_g)/\phi_g$. Thus $+$ $(-)$ refer to the non-ergodic (ergodic) side. On the macroscopic time scale $\tau \sim \tau_\alpha$, the dynamics on the ergodic or fluid side of the transition are governed by the α process for which the theory predicts another scaling law,

$$f(q,\tau) = f_c(q)\exp(-\tau/\tau_\alpha)^\gamma \tag{14}$$

The α process is a slow process that is arrested in the non-ergodic phase and only the β process persists.

On the ergodic side ($\phi < \phi_g$), the single exponential decay in $f(q,\tau)$ up to $\phi/\phi_g = 0.89$ is in agreement with MCT predictions of a single step decay up to $\phi/\phi_g = 0.9$.[18,25] Experiments closer to the gel line on the ergodic side, where perceptible multiple step decays of $f(q,\tau)$ have been predicted by the MCT, have not been performed on our system.

We note that the observations of single exponential decays of $f(q,\tau)$ are qualitatively different from the experiments of Solomon and Varadan,[14] who find stretched exponential relaxations of $f(q,\tau)$ in their ergodic and non-ergodic samples at the shortest measurable timescales. These latter experiments are in agreement with the experiments of Krall and Weitz,[29] who investigated the dynamics of structural relaxation of the interiors of clusters that constituted gels.

In Fig. 6, for $\phi > \phi_g$, we show the fits of MCT using eqns. (11), (12) and (13) to our experimental data on the non-ergodic side. A short time exponential decay of $f(q,\tau)$, with $\Gamma = q^2 D$, is followed by a slow two-step decay to a plateau over a relatively large τ window. We emphasize that in agreement with MCT, D is independent of q and for this sample takes on a value of 1.1×10^{-7} cm^2 s^{-1} ($D/D_0 \sim 0.1$).

MCT describes suspensions with particles experiencing centrosymmetric attractions and predicts a smooth decay to an intermediate plateau. For purposes of comparison, we ignore the two-step decay and find that the data is captured quite well by the MCT power-law β correlator, with the

characteristic relaxation time, τ_β, independent of q and the non-ergodicity parameter, $f_c(q)$, decreasing with increasing q. In the curve fits, independent of q the best fit is found with $a = 0.3$.

We further test the scaling behavior of the relaxation time, τ_β, with the volume fraction by plotting τ_β as a function of the separation parameter, $\chi = \phi/\phi_g - 1$ (inset of Fig. 6). The values of τ_β show a power law divergence with $\tau_\beta \sim \chi^{-1.8}$. The MCT prediction for the exponent for τ_β is $-1/2a = -1.66$.[18] The close agreement of the experimental and predicted power law exponents provides a reassuring consistency check on the MCT predictions.

The internally consistent agreement of the MCT predictions with our experiments suggests that gelation in our system corresponds to the slowing down of structural relaxation, due to the increasing rigidity of the percolated network of particles, rather than the percolation of clusters. However, that clusters could precede the formation of the percolated network cannot be ruled out. Segre *et al.*[15] estimate an average cluster size, R, in their gelled suspensions using $\phi_g(2R/\sigma)^{3-d} = 1$, where d is the cluster fractal dimension, and ϕ_g, the particle volume fraction at gelation. Assuming $d = 2$ and for $\phi_g = 0.074$, we find that at gelation $R/\sigma \sim 5$. Our light scattering experiments have been performed in the regime $0.02 < \sigma q < 0.1$, which allows clusters of sizes $30 < R/\sigma < 200$ to be seen. Thus, clusters, even if they existed, would not be detected from the static light scattering experiments. On the other hand, if clusters of size (30–200)σ were in solution at any appreciable concentration below ϕ_g, we would expect to see this reflected in $f(q,\tau)$ as multiple exponential decays. This was not observed indicating that clusters, if formed, grow only for $\phi/\phi_g > 0.89$.

The two-step decay in $f(q,\tau)$ may arise from the anisotropic interactions. When particles experience anisotropic interactions, constraints on particle motion other than diffusion within and out of cages become possible. Particles are not only localized in cages, but are restricted to specific orientations within these cages due to the anisotropic nature of their interactions. Thus, after an extremely short diffusive excursion due to its interactions with the solvent, an anisotropically bound particle experiences orientational constraints to its motion. This causes the additional plateau in $f(q,\tau)$ observed in our experiments leading to the two-step decay. Breaking the anisotropic bonds allows further excursions causing $f(q,\tau)$ to decay further. The particle then encounters the cage and a second plateau in $f(q,\tau)$ results. Finally, cooperative rearrangement causes cage break-up leading to the final decay of $f(q,\tau)$. Experiments on gelling systems where anisotropy in interparticle interactions are varied systematically would aid development of models to describe such phenomena.

V. Percolation, gelation and crystallization

Several studies of gelling systems indicate that increasing either the particle volume fraction or the strength of attraction of colloidal particles results in an increasing tendency of the system to form gels.[3–8,14–16] In contrast, for the lysozyme/phosphate system we find that while increasing particle volume fraction increases the tendency to form gels, increasing the strength of attraction at a fixed volume fraction increases the tendency of the system to crystallize. We hypothesize that the surprising appearance of crystals at lower volume fractions and larger strengths of attraction is the consequence of a combination of the slow crystallization kinetics and the location of the gel line.

Consider a system that cannot crystallize (by having, for example, too wide a particle size distribution), which experiences short range attractions. With increasing volume fraction and increasing strength of attraction, this system will display a fluid–fluid phase boundary. However, at strengths of attraction typically smaller than that at the critical point and at volume fractions typically above the critical volume fraction, there is a percolation boundary where clusters arising from thermal fluctuations first percolate through the suspension. We refer to this as the static percolation boundary. System dynamics and osmotic compressibility change smoothly through the percolation boundary. The infinite clusters first seen at the static percolation boundary have only instantaneous life times. However, as the volume fraction moves above the percolation boundary, particles find themselves in cages that rearrange more slowly, the life times of the infinite clusters increase, with the result ultimately being glass or gel formation.

At any given strength of attraction, let ϕ_{MCT} denote the volume fraction where MCT predicts gelation, and let ϕ_{sp} be the static percolation boundary. MCT predicts when "bonds" are formed such that particles cannot diffuse apart. Thus, non-ergodic dynamics will be observed for

$\phi > \phi_{MCT}$. Similarly, a percolated network of particles begins to exist in the suspension for $\phi > \phi_{sp}$. Depending on the relative locations of the gel and percolation boundaries, two scenarios are possible: When $\phi > \phi_{MCT} > \phi_{sp}$, space filling networks are formed that are non-ergodic. However, for $\phi_{MCT} < \phi < \phi_{sp}$, MCT models predict the formation of long lived clusters. These clusters will be internally non-ergodic but the cluster centers of mass will remain ergodic (reminiscent of the ergodic gels discussed by Segre *et al.*[15]).

In the latter case, macroscopic gels will be observed at volume fractions where the non-ergodic clusters percolate, which can be significantly higher than ϕ_{MCT}. As a result, in this case MCT is expected to underpredict the gel volume fraction. That MCT is able to predict the gel volume fractions at all strengths of attraction in our experiments suggests that $\phi_{MCT} > \phi_{sp}$ under these conditions. Indeed, light scattering experiments also show no evidence of (non-ergodic) cluster formation at volume fractions very close to the gel boundary.

If we now allow the particles to crystallize (by working with the same short range attraction but reducing the spread in the particle size distribution), a different type of fluctuation leading to crystals may occur in the suspension. The driving force for crystal formation and the rate of crystal nucleation grow as ϕ/ϕ_{sat} increases above unity. If the gel boundary occurs below the solubility curve, gelation will only occur if non-ergodic structures form faster than crystals nucleate and grow; otherwise, crystals will be observed.

We therefore argue that in our experiments, gels occur upon crossing the MCT gel boundary (since $\phi_{MCT} > \phi_{sp}$), under conditions where the driving force for crystal nucleation is small. This occurs at small strengths of attraction. At higher strengths of attraction, the driving force for crystal nucleation reaches sufficient levels for $\phi < \phi_{MCT}$ that crystals form before gelation.

We illustrate these ideas with the phase behavior of square well particles shown in Fig. 7 where we have plotted predictions of the solubility boundary from a square well equation of state with $\Delta = 0.08$. To determine the thermodynami properties of the fluid state we use an equation of state which captures machine calculations on square well fluids to within 10%:[30,31]

$$\frac{Pa^3}{\phi kT} = \frac{3}{4\pi}\left[1 + \frac{4\phi}{(1-1.19\phi)^2} + \frac{6}{\pi}\frac{(\varepsilon/kT)\phi h(\Delta)}{\left(1-\frac{\phi}{\phi_b}\right)^3}\right] \tag{15}$$

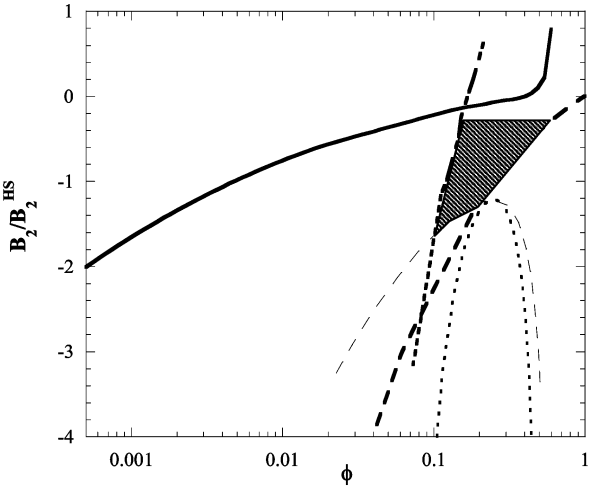

Fig. 7 Calculations of the equilibrium and non-equilibrium phase boundaries for square well systems. The solid line indicates the fluid–solid boundary for a square well fluid at $\Delta = 0.08$. The dot–dashed line represents square well ($\Delta = 0.2$) percolation boundary[24] and is extrapolated (short dashed line) to higher strengths of attraction. The long dashed line represents the MCT bond formation line at $\Delta = 0.08$. The thin dashed and dotted lines represent the binodal and spinodal for $\Delta = 0.08$.

where P is the osmotic pressure, ϕ, the particle volume fraction, and ϕ_b and $h(\Delta)$ are both tabulated functions of Δ. From this, the chemical potential of a particle in the fluid phase is calculated as

$$\mu_l = \int_0^{\phi} \left(\frac{4\pi}{3} \frac{Pa^3}{\phi' kT} - 1 \right) \frac{\mathrm{d}\phi'}{\phi'} + \frac{4\pi}{3} \frac{Pa^3}{\phi kT} + \ln(\phi) - 1 \tag{16}$$

The fluid–fluid phase separation boundary, or the binodal, is determined using the conditions, $P^{\mathrm{I}} = P^{\mathrm{II}}$ and $\mu_l^{\mathrm{I}} = \mu_l^{\mathrm{II}}$, where I and II correspond to the dilute and the dense fluid phases in equilibrium. The locus of points that satisfy $\mathrm{d}P/\mathrm{d}\phi = 0$ gives the spinodal. The spinodal and the binodal meet at the critical point. The fluid–crystal phase boundary, or the solubility boundary, is determined by the condition $\mu_{\mathrm{l}} = \mu_{\mathrm{s}}$, where μ_{s} is the chemical potential of a particle in the crystalline phase, calculated as

$$\mu_{\mathrm{s}} = -C\varepsilon/2kT - 3\ln(\Delta) \tag{17}$$

where $C = 12$ is the number of nearest neighbors of particles in the crystalline phase, and the solid is assumed to be incompressible. Shown in Fig. 7 as a solid line are calculations of the solubility boundary for $\Delta = 0.08$ (for which $h(\Delta) = -2.724$ and $\phi_{\mathrm{b}} = 1.482$). Under these conditions, the critical point occurs at $(B_2/B_2^{\mathrm{HS}})_{\mathrm{c}} = -1.2$ and $\phi_{\mathrm{c}} = 0.25$. A comparison of the predicted and measured inverse osmotic compressibilities, $1/S(0)$ or $(\mathrm{d}P/kT\mathrm{d}\rho)$, is shown in Fig. 2. The inability of the square well model to predict the critical point is emphasized in this system where the predicted square well spinodal occurs at $\phi = 0.082$ at 10 °C, while the experimental data demonstrate that the system lies above the critical point under these conditions. Better agreement can be found by assuming that the particles experience anisotropic interactions.[2,12]

Also shown in Fig. 7 are the MCT gel line and the predictions of the static percolation line developed by Chiew and Glandt[22] for $\Delta = 0.2$. The static percolation boundary is expected to move to the left in the figure as Δ is reduced (Chiew and Glandt[22] report numerical calculations of the percolation line only at $\Delta = 0.2$ and 0.5).

Clearly, regions exist in the phase diagram where $\phi_{\mathrm{MCT}} > \phi_{\mathrm{sp}}$. The portion of this region away from the metastable fluid–fluid region is shown shaded, and we expect our experimental conditions to be in an analogous region on the phase diagram for anisotropic potentials. In this region, gels predicted by MCT would occur for $\phi > \phi_{\mathrm{MCT}}$. We also note that the MCT gel line and the solubility boundary have different dependences on the strength of attraction. As the strength of attraction increases, ϕ_{sat} decreases much more than ϕ_{MCT}. As a result, the driving force for crystal nucleation increases much more than the driving force for gelation upon increasing the strength of attraction at a given ϕ. Thus, at small strengths of attraction, gelation is observed before (at lower volume fractions than) crystallization, and at higher strengths of attraction, crystallization occurs before gelation. The crossover is seen in our experiments at $B_2/B_2^{\mathrm{HS}} \sim -2.5$.

VI. Conclusions

The lysozyme/phosphate systems explored here exhibit very slow crystal nucleation kinetics. As a consequence, the dynamics of density fluctuations in supersaturated fluids can be explored. Gels are observed in this metastable region when the gel line lies sufficiently close to the fluid–crystal phase boundary that crystal nucleation does not mask the formation of the gel. At larger strengths of attraction and lower volume fractions, crystals form faster than gelation can be observed. Mode coupling theory predictions of the gel boundary are found to be quite accurate for those systems where crystallization does not mask gelation. Predictions of the dynamics of gelation are also in excellent agreement with the experiments, suggesting that gelation in protein systems is described well by MCT.

We hypothesize that gelation occurs at volume fractions predicted by MCT when the MCT gel line lies at volume fractions above the static percolation boundary. For systems where the MCT gel line occurs at volume fractions lower than the percolation boundary, ergodic gels may be observed. In either case, crystals may be observed if the kinetics of crystal nucleation is faster than the kinetics of forming non-ergodic clusters. We conclude that the competition between gelation and crystallization will depend on the relative locations of the percolation, gel and solubility

boundaries. Further support for our hypothesis requires the development of descriptions for percolation and non-ergodic transitions for particles experiencing anisotropic interactions and experiments on systems with better defined pair potentials.

Acknowledgements

The authors thank M. Fuchs and K. Schweizer for their many insightful comments. Support from the U.S. DOE *via* the University of Illinois at Urbana-Champaign, Frederick Seitz Materials Research Laboratory, Grant No. DEFG0296ER45439 is gratefully acknowledged.

References

1 W. B. Russel, D. A. Saville and W. R. Schowalter, *Colloidal Dispersions*, Cambridge University Press, Cambridge, 1989.
2 A. M. Kulkarni, PhD Thesis, University of Illinois, 2001.
3 S. M. Ilett, A. Orrock, W. C. K. Poon and P. N. Pusey, *Phys. Rev. E*, 1995, **51**, 1344.
4 N. A. M. Verhaegh, D. Asnaghi, H. N. W. Lekkerkerker, M. Giglio and L. Cipelletti, *Physica A*, 1997, **242**, 104.
5 J. W. Jansen, C. G. de Kruif and A. Vrij, *J. Colloid Interface Sci.*, 1986, **114**, 481.
6 M. C. Grant and W. B. Russel, *Phys. Rev. E*, 1993, **47**, 2606.
7 H. Verduin and J. K. G. Dhont, *J. Colloid Interface Sci.*, 1995, **172**, 425.
8 (*a*) C. J. Rueb and C. F. Zukoski, *J. Rheol.*, 1997, **41**, 197; (*b*) C. J. Rueb and C. F. Zukoski, *J. Rheol.*, 1998, **42**, 1451.
9 D. F. Rosenbaum, P. C. Zamora and C. F. Zukoski, *Phys. Rev. Lett.*, 1996, **76**, 150.
10 M. Muschol and F. Rosenberger, *J. Chem. Phys.*, 1997, **107**, 1953.
11 A. Lomakin, N. Asherie and G. B. Benedek, *Proc. Natl. Acad. Sci., USA*, 1999, **96**, 9465.
12 R. P. Sear, *J. Chem. Phys.*, 1999, **111**, 4800.
13 D. F. Rosenbaum, A. Kulkarni, S. Ramakrishnan and C. F. Zukoski, *J. Chem. Phys.*, 1999, **111**, 9882.
14 M. J. Solomon and P. Varadan, *Phys. Rev. E*, 2001, **63**, 51 402.
15 P. N. Segre, V. Prasad, A. B. Schofield and D. A. Weitz, *Phys. Rev. Lett.*, 2001, **86**(26), 6042.
16 S. Ramakrishnan, M. Fuchs, K. S. Schweizer and C. F. Zukoski, *J. Chem. Phys.*, submitted.
17 (*a*) P. N. Pusey and W. van Megen, *Physica A*, 1989, **157**, 705; (*b*) P. N. Pusey and W. van Megen, *Phys. Rev. Lett*, 1987, **59**, 2083.
18 (*a*) J. Bergenholtz and M. Fuchs, *Phys. Rev. E*, 1999, **59**, 5706; (*b*) J. Bergenholtz and M. Fuchs, *J. Phys.: Condens. Matter B*, 1999, 10 171.
19 A. J. Sophianopoulos, C. K. Rhodes, D. N. Holcomb and K. E. van Holde, *J. Biol. Chem.*, 1962, **237**, 1107.
20 A. M. Kulkarni, A. P. Chatterjee, K. S. Schweizer and C. F. Zukoski, *J. Chem. Phys.*, 2000, **113**, 9863.
21 J. L. Harland and W. van Megen, *Phys. Rev. E*, 1997, **55**, 3054.
22 Y. C. Chiew and E. D. Glandt, *J. Phys. A*, 1983, **16**, 2599.
23 M. G. Noro, N. Kern and D. Frenkel, *Europhys. Lett.*, 1999, **48**, 332.
24 Z. Cheng, J. Zhu, W. B. Russel, W. V. Meyer and P. M. Chaikin, *Appl. Opt.*, 2001, **40**, 4146.
25 J. Bergenholtz, M. Fuchs and Th. Voightmann, *J. Phys.: Condens. Matter*, 2000, **12**, 6575.
26 S. Beretta, G. Chirico and G. Baldini, *Macromolecules*, 2000, **33**, 8663.
27 B. M. Fine, A. Lomakin, O. O. Ogun and G. B. Benedek, *J. Chem. Phys.*, 1996, **104**, 326.
28 N. M. Dixit and C. F. Zukoski, *J. Colloid Interface Sci.*, 2000, **228**, 359.
29 A. H. Krall and D. A. Weitz, *Phys. Rev. Lett. B*, 1998, 778.
30 S. Ramakrishnan and C. F. Zukoski, *J. Chem. Phys.*, 2000, **113**(3), 1237.
31 A. M. Kulkarni and C. F. Zukoski, *Langmuir*, 2002, **18**, 3090.